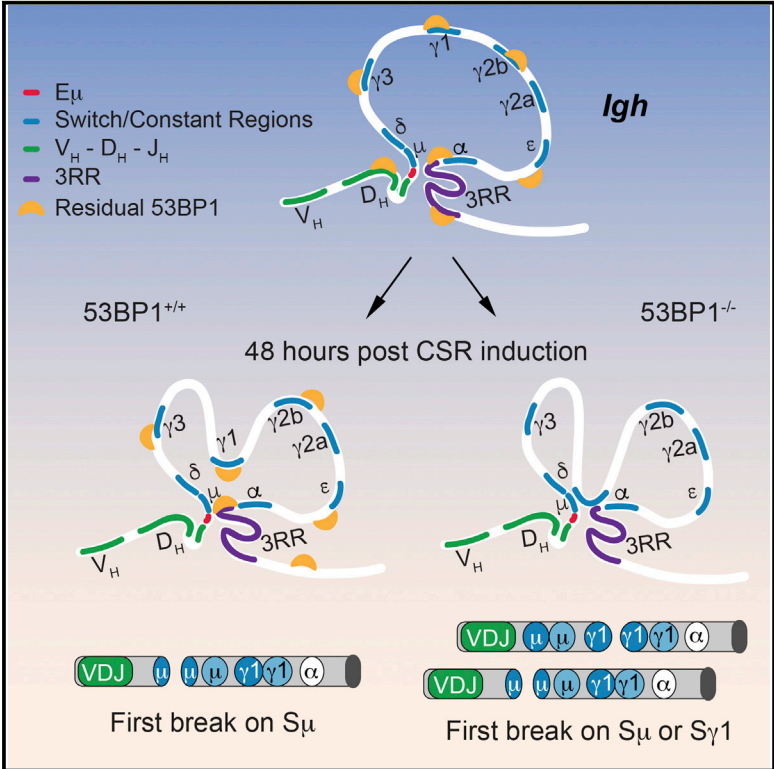


# Cell Reports

## A Damage-Independent Role for 53BP1 that Impacts Break Order and *Igh* Architecture during Class Switch Recombination

### Graphical Abstract



### Authors

Pedro P. Rocha, Ramya Raviram, Yi Fu, ..., John Petrini, Gunnar Schotta, Jane A. Skok

### Correspondence

pereip02@nyumc.org (P.P.R.), jane.skok@nyumc.org (J.A.S.)

### In Brief

Rocha et al. describe a role for the DNA-damage sensor 53BP1 that is independent of the DNA double-strand break repair pathway. Residual recruitment of 53BP1 to chromatin impacts the 3D structure of *Igh* during CSR and is necessary for ordered AID-mediated break formation on switch regions.

### Highlights

- 53BP1 is essential for preferential targeting of the upstream switch region
- 53BP1’s absence results in increased interaction frequency between switch regions
- Alterations in switch region targeting and locus architecture impact CSR
- 53BP1’s action is independent of its role in the double-strand break repair pathway

### Accession Numbers

GSE81180



# A Damage-Independent Role for 53BP1 that Impacts Break Order and *Igh* Architecture during Class Switch Recombination

Pedro P. Rocha,<sup>1,\*</sup> Ramya Raviram,<sup>1,2</sup> Yi Fu,<sup>1</sup> JungHyun Kim,<sup>1</sup> Vincent M. Luo,<sup>1</sup> Arafat Aljoufi,<sup>1</sup> Emily Swanzey,<sup>3</sup> Alessandra Pasquarella,<sup>4</sup> Alessia Balestrini,<sup>5</sup> Emily R. Miraldi,<sup>7</sup> Richard Bonneau,<sup>2,6,7</sup> John Petrini,<sup>5</sup> Gunnar Schotta,<sup>4</sup> and Jane A. Skok<sup>1,\*</sup>

<sup>1</sup>Department of Pathology, New York University School of Medicine, New York, NY 10016, USA

<sup>2</sup>Department of Biology, New York University, New York, NY 10003, USA

<sup>3</sup>Department of Developmental Genetics, New York University School of Medicine, New York, NY 10016, USA

<sup>4</sup>Ludwig Maximilians University and Munich Center for Integrated Protein Science (CiPSM), Biomedical Center, Planegg-Martinsried 80336, Germany

<sup>5</sup>Molecular Biology Program, Memorial Sloan Kettering Cancer Center, New York, NY 10065, USA

<sup>6</sup>Department of Computer Science, Courant Institute of Mathematical Sciences, New York, NY 10012, USA

<sup>7</sup>Simons Center for Data Analysis, New York, NY 10010, USA

\*Correspondence: [pereip02@nyumc.org](mailto:pereip02@nyumc.org) (P.P.R.), [jane.skok@nyumc.org](mailto:jane.skok@nyumc.org) (J.A.S.)

<http://dx.doi.org/10.1016/j.celrep.2016.05.073>

## SUMMARY

During class switch recombination (CSR), B cells replace the *Igh* C $\mu$  or  $\delta$  exons with another downstream constant region exon (C $H$ ), altering the antibody isotype. CSR occurs through the introduction of AID-mediated double-strand breaks (DSBs) in switch regions and subsequent ligation of broken ends. Here, we developed an assay to investigate the dynamics of DSB formation in individual cells. We demonstrate that the upstream switch region S $\mu$  is first targeted during recombination and that the mechanism underlying this control relies on 53BP1. Surprisingly, regulation of break order occurs through residual binding of 53BP1 to chromatin before the introduction of damage and independent of its established role in DNA repair. Using chromosome conformation capture, we show that 53BP1 mediates changes in chromatin architecture that affect break order. Finally, our results explain how changes in *Igh* architecture in the absence of 53BP1 could promote inversional rearrangements that compromise CSR.

## INTRODUCTION

Class switch recombination (CSR) is dependent on the cytidine deaminase enzyme (AID), which initiates the formation of two double-strand breaks (DSBs) within the switch regions of *Igh* that precede each C $H$ . The broken ends are then joined by members of the non-homologous end joining (NHEJ) pathway, placing a new C $H$  exon in front of the V(D)J exons (Keim et al., 2013; Stavnezer and Schrader, 2014). This occurs through preferential joining of proximally located DSBs on the same chromo-

some (Gostissa et al., 2014). CSR is distinct from other recombination events that join two DSBs where ligation can either result in a deletional event or inversion of the intervening sequence (Dong et al., 2015). What makes CSR special is that somehow, through an unknown mechanism that is dependent on the DNA-damage pathway effector 53BP1, break repair is strongly biased toward deletional joining, thereby increasing the efficiency of the process (Di Noia, 2015; Dong et al., 2015).

The introduction of I-SceI sites in place of switch regions results in an increase in the frequency of inversional events. This demonstrates that the switch regions themselves are important for the bias toward deletional joining (Dong et al., 2015). Because I-SceI breaks are likely to occur simultaneously and at a similar frequency on the two sites, they do not reflect the dynamics of AID-mediated breaks on switch regions, which are presumed to occur at different rates and in a particular order, with the upstream S $\mu$  site being targeted first (Chaudhuri et al., 2004). This suggests that break order might be an important determinant for successful deletional CSR. In addition, the fact that rare inter-chromosomal *Igh* rearrangements involving switch regions do not share a deletional bias (Dong et al., 2015) points to a role for chromatin architecture of the *cis* allele favoring deletional events. However, there have been no studies that examine break order or chromatin architecture of *Igh* and the impact of 53BP1 in either context.

The first studies investigating the dynamics of DSB formation during CSR indicate that AID targeting of S $\mu$  occurs independently and at higher frequency than targeting of the downstream switch region (Dudley et al., 2002; Gu et al., 1993; Schrader et al., 2003; Zhang et al., 2010). Other studies using I-SceI-introduced DSBs in the *Myc* locus demonstrate that AID-induced translocations to the *Igh* S $\mu$  region (Chiarle et al., 2011; Hu et al., 2014; Klein et al., 2011) occur at a 2-fold increased rate compared to downstream switch regions, a much lower frequency than that expected from mutation rate differences in each location (Dudley et al., 2002; Schrader et al., 2003). The discrepancy between

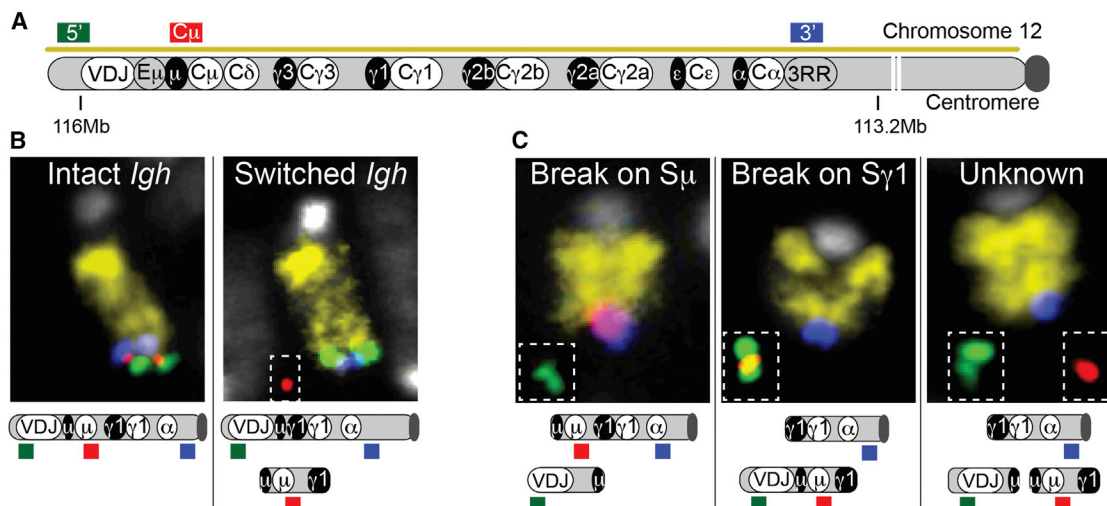


**Figure 1. A Single-Cell System to Study the Dynamics of Break Order during CSR**

(A) Scheme of the *Igh* locus and location of *Igh*-specific probes used in the study. Switch and constant regions are represented as black and white ovals, respectively. Mouse chromosome 12 is identified by a yellow chromosome paint.

(B) Example of chromosome 12 with an unswitched (left) and switched *Igh* allele (right) is shown.

(C) Examples of *Igh* alleles with break first on  $S_{\mu}$  (left),  $S_{\gamma 1}$  (center), or unknown (right). Broken signals shown as dashed insets are placed next to the chromosome of origin for clarity. Full pictures of the cells where these examples were captured can be found in [Figure S1](#).

these results might arise from the fact that these studies were based on analyses of populations of cells and, therefore, do not provide information about the dynamics of DSB introduction in single cells. To address this issue, we used a single-cell metaphase-based fluorescence in situ hybridization (FISH) assay to study the dynamics of AID-mediated DSB introduction on *Igh* switch regions.

## RESULTS

### A Single-Cell System to Study the Order of DSB Formation during CSR

For our assay, we prepared metaphase spreads after 60–65 hr of B cell activation using  $\alpha$ CD40 and IL4 to induce IgG1 switching. We used a mixture of four differentially labeled DNA probes, which included a mouse chromosome 12 paint (to identify the chromosome containing *Igh*), two locus-specific probes that hybridize to the region immediately surrounding the *Igh* locus (named 5' and 3' probes), and a probe that hybridizes to the region between  $S_{\mu}$  and  $S_{\gamma 3}$  (named the  $C_{\mu}$  probe) (Figure 1A). An *Igh*-switched allele was identified by loss of the  $C_{\mu}$  signal on chromosome 12 (Figures 1B and S1A). Using this system, we were able to accurately examine switching in an allele-specific manner, and we found that the level at which switching occurred was compatible with that detected by fluorescence-activated cell sorting (FACS) analysis (Table S1).

The DNA probes we designed can also be used to detect CSR-related chromosomal abnormalities on the *Igh* locus. As a proof of principle, we activated splenic B cells in the presence of an inhibitor of ATM kinase (ATMi), which is known to increase chromosomal abnormalities in the *Igh* locus due to its contribution to DSB repair and activation of cell cycle checkpoints (Reina-San-Martin et al., 2004). As previously reported (Franco et al.,

2006), the most frequent chromosomal abnormality on the *Igh* locus was the separation of its ends such that the *Igh* 5' telomeric probe and the *Igh* 3' signal were no longer found together on chromosome 12 (split ends) (Figure S1B; Table S2). In addition, we detected frequent *Igh* translocations with loci on other chromosomes as well as translocations between the two alleles of chromosome 12. The latter form dicentric chromosomes that retain the 3' probe (Franco et al., 2006). Finally, we also detected frequent breaks on chromosome 12 that occurred centromeric to the *Igh* locus, as has been described previously in ATM-deficient B cells (Hu et al., 2014).

To investigate the order that DSBs are introduced during CSR, we focused on cells where the 5' and 3' probes were no longer together at the telomeric end of chromosome 12 (*Igh* split ends category). It should be noted that this type of damage results from AID-induced breaks on switch regions, as it is not detected in AID-deficient cells (*Aicda*<sup>-/-</sup>) (Figure S1B). In cells activated to undergo IgG1 switching, chromosomes that retained the  $C_{\mu}$  probe on chromosome 12 next to the *Igh* 3' probe allowed us to infer that the break occurred at  $S_{\mu}$ , while  $S_{\gamma 1}$  was still intact (Figure 1C, left and Figure S1C). On the other hand, if the  $C_{\mu}$  probe was associated with the 5' probe and both were separated from chromosome 12, we could conclude that the break occurred first on  $S_{\gamma 1}$  (Figure 1C, middle). Finally, in cells where the  $C_{\mu}$  probe was separated from the 5' probe and both were separated from chromosome 12, we could not identify the location of the first break and we classified these as unknown (Figure 1C, right). As the  $C_{\mu}$  probe is located upstream of  $S_{\gamma 3}$ , this same system could also be applied to lipopolysaccharide (LPS) activation, which induces switching to IgG3 and IgG2a, or to CH12 cells activated in the presence of  $\alpha$ CD40, IL4, and TGF- $\beta$  to undergo IgA switching (Figure S1A).

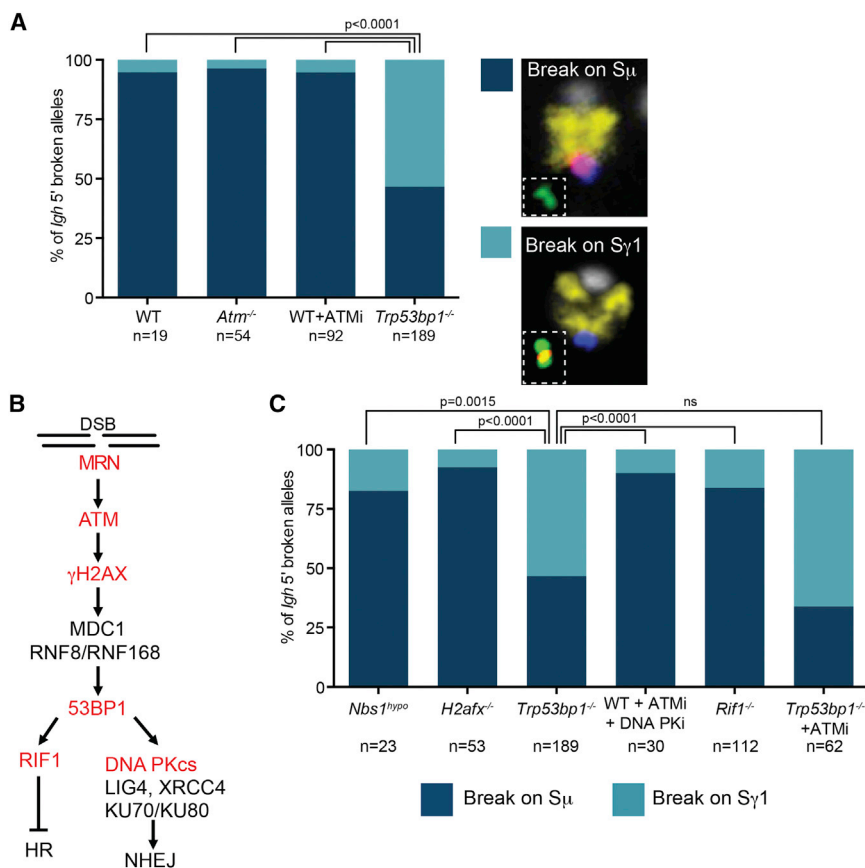


**Figure 2. 53BP1 Determines Break Order Independently of the DNA Damage Pathway**

(A and C) *Igh* alleles where location of the first break can be determined were divided into break-first-on-S $\mu$  or -S $\gamma$ 1 categories for the different mutants or treatments. Next to plots, the same examples as in Figure 1 are shown for representative images for each category. Pictures of full cells can be seen in Figure S1. Significance was calculated using Fisher's exact test. Table S3 details the number of replicates and alleles analyzed. Plots represent the average frequency of each category across replicate experiments. N represents the number of *Igh* alleles where break order could be determined across all replicates analyzed.

(B) Scheme shows the DSB repair pathway that is active during CSR.

of B cells deficient for H2AX (*H2afx*<sup>-/-</sup>) or expressing a hypomorphic NBS1 (*Nbs1*<sup>hyp</sup>) showed that these cells were able to maintain a wild-type phenotype with respect to break order (Figures 2B and 2C). This is a surprising result because  $\gamma$ H2AX and the MRN complex (composed of MRE11, NBS1, and RAD50) are necessary for recruitment of 53BP1 following the introduction of DSBs on *Igh* (Panier and Boulton, 2014; Reina-San-Martin et al., 2004).

To determine whether 53BP1's role in inhibiting resection is an important factor

### A 53BP1-Dependent Mechanism Ensures Targeting of S $\mu$

We analyzed the location of breaks during CSR in B cells derived from wild-type mice, ATM-deficient mice (*Atm*<sup>-/-</sup>), and wild-type B cells treated with an ATM kinase inhibitor. Across the three conditions, S $\mu$  was the first switch region to be targeted in more than 95% of the chromosomes where break location could be determined (Figure 2A; Table S3). These results are in line with analysis of mutation rates that show that S $\mu$  is targeted at a higher frequency than downstream switch regions (Dudley et al., 2002; Reina-San-Martin et al., 2007; Schrader et al., 2003).

Given 53BP1's unique role in biasing toward deletional recombination events, we next asked whether 53BP1 could influence DSB introduction. Indeed, in B cells deficient for 53BP1 (*Trp53bp1*<sup>-/-</sup>), the mechanism ensuring that breaks are introduced first on S $\mu$  is lost and the first break is introduced randomly at S $\mu$  and S $\gamma$ 1 (Figure 2A). This mechanism is not specific for IgG1 switching, as the same effect was detected in cells activated with LPS (that switch to IgG3 and IgG2a) as well as in the CH12 cell line (where switching to IgA occurs) (Figure S2A).

### 53BP1 Impacts DSB Introduction Independently of the DNA Damage Pathway

Given our finding that 53BP1 is important for ensuring break order, we next asked whether proteins involved in 53BP1 recruitment also impact the dynamics of DSB introduction. Analysis

in determining break order, we next analyzed metaphase spreads from RIF1-deficient B cells (*Rif1*<sup>-/-</sup>). 53BP1 recruits RIF1 in an ATM-dependent manner to inhibit resection of the switch regions and recruitment of BRCA1 (Panier and Boulton, 2014). Our results clearly indicate that B cells deficient in RIF1 did not recapitulate the defect in break order that was found in 53BP1 mutant B cells (Figures 2B and 2C). Finally, we examined activated B cells treated with a combination of ATMi and DNA PK inhibitors that prevent NHEJ repair (Callén et al., 2009). Once again, we found that the cells exhibited a wild-type phenotype for break order. Together, these data suggest that the mechanism by which 53BP1 impacts the choice of break order occurs independently of the MRN-ATM- $\gamma$ H2AX pathway and its known role in DNA repair.

### Altered DSB Dynamics in the Absence of 53BP1 Is Not Due to an Accumulation of DSBs in S $\gamma$ 1

Given that AID-mediated breaks are introduced during the G1 phase of the cell cycle, it could be argued that the defect in break order in 53BP1-deficient cells results from an accumulation of DSBs in S $\gamma$ 1 that are more difficult to repair. However, if that were the case, slower repair would increase the chances of breaks in both switch regions, thereby increasing the number of cells in the unknown category, which we did not observe (Table S3). Moreover, cells deficient in proteins upstream (ATM,  $\gamma$ H2AX, and MRN) or downstream (RIF1 and DNA PKcs) of 53BP1 in the DNA-damage repair pathway do

not show the same phenotype as 53BP1-deficient cells. Thus, if the DSBs in  $S_{\gamma 1}$  were caused by an accumulation of difficult-to-repair breaks, the 53BP1 phenotype should be recapitulated in these other models. That this was not the case indicates that the 53BP1 phenotype is not an artifact caused by a defect in DNA repair. Additionally, we can rule out that the 53BP1 effect is related to an increase in resection, since we did not detect the same phenotype in RIF1-deficient cells. Moreover, inhibition of ATM in 53BP1-deficient cells, which prevents resection (Bunting et al., 2010; Dong et al., 2015), did not change the distribution of where breaks were introduced first (Figures 2B and 2C). Given that ATMi blocks activation of cell cycle checkpoints, this result also suggests that the breaks we detected did not result from differences in the ability of the mutant cells to activate cell cycle checkpoints or a downstream accumulation of damage.

To further validate that the phenotype we observed in cells deficient for 53BP1 was not caused by the accumulation of  $S_{\gamma 1}$  breaks that are difficult to repair, we repeated the assay at different time points (48, 72, and 96 hr of activation) using wild-type B cells treated with an ATMi as well as B cells from 53BP1-deficient mice. At 48 hr, cells deficient for 53BP1 already displayed the same phenotype we observed at later time points, where the initial DSB could be found at the same frequency in  $S_{\mu}$  and  $S_{\gamma 1}$  (Figure S2B). As AID-induced breaks only start to accumulate following 48 hr of activation (Schrader et al., 2005), this provides further support that the phenotype is not an artifact caused by the accumulation of breaks.

### Residual Binding of 53BP1 to Chromatin Independent of Damage Determines DSB Introduction

Our results indicate that 53BP1 ensures break order independently of its role in DNA repair. Residual binding of 53BP1 to chromatin has been shown to occur throughout the genome independent of DNA damage (Bekker-Jensen et al., 2005; Bohgaki et al., 2013; Bothmer et al., 2011; Santos et al., 2010). Binding relies on the histone mark H4K20me<sub>2</sub>, which is recognized by the TUDOR domain of 53BP1. This modification is deposited by the SUV4-20H1/H2 enzymes, and, in SUV4-20H1/H2-deficient cells, 90% of the methylated H4K20 is converted to the mono-methyl state (Schotta et al., 2008). CSR efficiency in these mutant B cells has been shown to be reduced by 50%, and there is accompanying damage detected on the *Igh* locus. Despite these findings, in mutant cells, recruitment of 53BP1 to sites of breaks occurs at high levels, albeit at a slower rate. Metaphase analysis of activated SUV4-20H1/H2-deficient splenic B cells (*Suv4-20h<sup>dm</sup>*) demonstrates that an absence of the di-methyl mark has no impact on the order of break introduction in the  $S_{\mu}$  and  $S_{\gamma 1}$  switch regions (Figure S2C). This result suggests that the TUDOR domain of 53BP1 can efficiently recognize the H4K20me<sub>1</sub> mark, a finding that supports previous observations (Botuyan et al., 2006; Oda et al., 2010).

The H4K20me<sub>1</sub> mark is deposited by the enzyme PR-SET7, which is essential for proliferation and cellular viability (Oda et al., 2010). It is therefore not possible to assess whether loss of the mono-methyl mark on H4K20 contributes to the 53BP1 phenotype of disrupted break order. However, a single amino acid mutation on the TUDOR domain of 53BP1 (*53BP1<sup>DR</sup>* mutant

mice) renders it unable to bind mono- or di-methylated H4K20 (Bekker-Jensen et al., 2005; Bothmer et al., 2011). Thus, analysis of activated splenic B cells isolated from these mice enabled us to address this question, and these cells fully recapitulated the phenotype of disrupted break order that we detected in 53BP1-deficient B cells (Figure S2C). Together these findings indicate that binding of 53BP1 to methylated H4K20 is important for determining break order, however, the di-methyl mark is dispensable for this function.

### 53BP1 Impacts the Architecture of *Igh* during CSR

Given that nuclear organization can have a dramatic impact on somatic recombination of antigen receptor loci (Chaumeil and Skok, 2012; Gerasimova et al., 2015), we asked whether a change in locus conformation could explain the alteration in break order on switch regions during CSR. It has previously been shown that an absence of 53BP1 does not result in dramatic changes in the *Igh* constant region of class switching B cells (Jankovic et al., 2013). To probe this further at a finer scale, we performed high-resolution circular chromosome conformation capture (4C-Seq). For this we used the 4-bp cutter enzyme DpnII as our primary restriction enzyme. Use of this frequent cutter enzyme increases resolution of interactions along the *Igh* locus 10-fold compared to 4C-seq libraries prepared with 6-bp cutters (Jankovic et al., 2013). Furthermore, 4C allows expansion of previous chromosome conformation capture (3C) analyses investigating *Igh* chromatin conformation (Feldman et al., 2015; Sellars et al., 2009; Wuerffel et al., 2007), by providing an unbiased assessment of relative interaction frequencies of all sites from a single viewpoint.

For 4C-seq experiments, we designed a bait located on the  $E_{\mu}$  enhancer, very close to  $S_{\mu}$  (Figures 3A and S3A). In resting cells (day 0),  $E_{\mu}$  interacts predominantly with the 3' regulatory region (3RR) enhancer, while the constant region exons between the two enhancers are extruded from this looping interaction. Analysis of Hi-C data, generated at high resolution in resting CH12-LX cells (Rao et al., 2014), confirms that, in resting cells, the *Igh* constant region is encompassed within a loop containing at its base the  $E_{\mu}$  and 3RR enhancers (Figures 3B and S3B). This structure resembles a topologically associated domain (TAD) (Nora et al., 2012) that is most likely to favor interactions between switch regions that are necessary for successful CSR.

According to our analysis, the  $S_{\gamma 1}$  region contacts the  $E_{\mu}$ -3RR loop base at increased frequency 48 hr after activation (a time when most breaks are being introduced). This is in line with previous 3C studies on the *Igh* locus (Wuerffel et al., 2007). Interestingly, in 53BP1-deficient cells, interaction of  $S_{\mu}$  with  $S_{\gamma 1}$  occurred at a significantly higher level (Figures 3A and S3A). Importantly, cells with combined AID and 53BP1 deficiency (*Trp53bp1<sup>-/-</sup>; Aicda<sup>-/-</sup>*) displayed the same interaction profile as cells deficient in 53BP1 alone. These findings provide the first evidence that 53BP1 has an impact on chromatin structure. That this effect occurs upstream of DNA damage is consistent with our finding that 53BP1 alters break order independently of the MRN-ATM- $\gamma$ H2AX pathway.

It is also interesting that, in contrast to previous studies (Feldman et al., 2015; Sellars et al., 2009; Wuerffel et al., 2007), we detected a slight reduction in the interaction between  $E_{\mu}$  and the

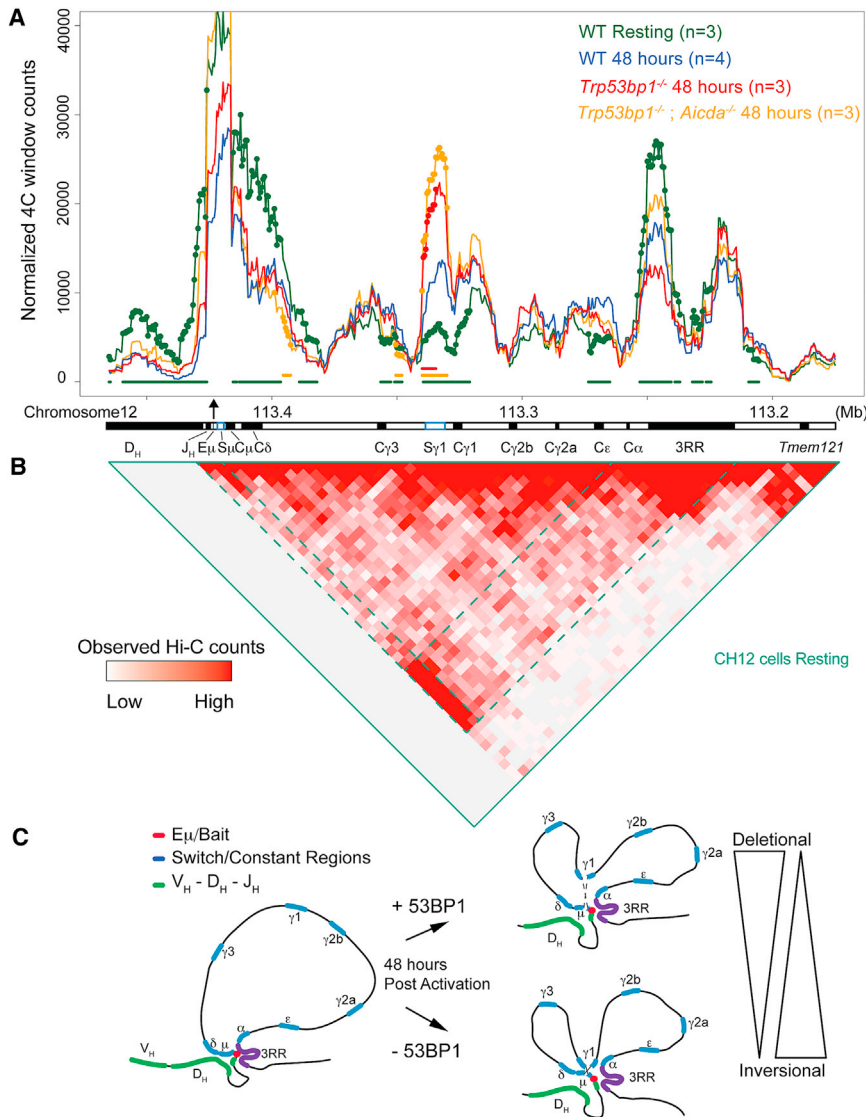


**Figure 3. 53BP1 Impacts the Architecture of *Igh* during CSR**

(A) 4C-seq using a bait (black arrow) located on the  $E_{\mu}$  enhancer. Lines represent the average 4C signal across replicates. Colored circles represent the 10-kb windows that have significant changes in contact frequency (adjusted p value < 0.05) from wild-type (WT) at 48 hr. For easier visualization, colored bars below lines represent consecutive windows that are statistically different from WT controls at 48 hr. For simplicity, only  $\mu$  and  $\gamma 1$  switch regions are shown (blue boxes). (B) Hi-C on the same region in CH12 cells. Dashed lines represent interactions between  $E_{\mu}$  and 3RR. Hi-C data are from the CH12 in-situ-combined track described in Rao et al. (2014). (C) Model shows changes in constant region locus conformation upon activation in WT and 53BP1-deficient cells and how these changes might favor inversional rearrangements.

two *Igh* enhancers ( $E_{\mu}$  and 3RR). In the absence of 53BP1, increased contact of  $S_{\gamma 1}$  with the enhancer hub is linked to the first break occurring randomly in  $S_{\mu}$  or  $S_{\gamma 1}$ . We propose that this change in chromosome looping exposes  $S_{\gamma 1}$  to the same high concentration of AID to which  $S_{\mu}$  is exposed, resulting in the first break being introduced as frequently in  $S_{\gamma 1}$  as in  $S_{\mu}$  (Figure 3C).

## DISCUSSION

In this study, we have developed an assay to investigate the order in which AID-mediated DSBs are introduced on *Igh* switch regions. Using this approach, we have shown that class switching B cells rely on a 53BP1-dependent mechanism that ensures the first break is introduced on the most upstream switch region ( $S_{\mu}$ ). Proteins involved in DSB repair and recruitment of 53BP1 to sites of damage do not contribute to break order regulation, suggesting that 53BP1 has a role in orchestrating CSR outside of its well-characterized function in DNA repair. It is tempting to speculate that failure to orchestrate appropriate break order could, in part, explain why 53BP1 mutant B cells have the lowest levels of switching compared to B cells deficient in other repair factors (Di Virgilio et al., 2013; Dong et al., 2015).

It is important to note that our assay cannot distinguish between breaks that would result in successful CSR from breaks that would be repaired within the same switch region and cause small internal deletions. We, therefore, assume that both these events have similar dynamics when it comes to targeting of switch regions by AID. We also cannot determine whether the number of breaks in each location is altered in the absence of 53BP1 or whether there is simply a change in the location of the first break. Analysis of AID-induced mutations in  $S_{\mu}$  suggests

3RR following 48 hr of activation. The interaction frequency was still high between  $E_{\mu}$  and 3RR, but lower than that seen for  $E_{\mu}$ - $C_{\gamma 1}$ . This discrepancy could result from different activation conditions:  $\alpha$ CD40 + IL4 versus LPS + IL4. When we used the same 4C primers in an experiment in which B cells were activated with LPS + IL4, we also found an increase in the interaction between  $E_{\mu}$  and the 3RR (Thomas-Claudepierre et al., 2016). It is known that activation under these conditions results in differences in targeting of switch regions: LPS with IL4 induces DSBs at  $S_{\gamma 3}$ ,  $S_{\gamma 1}$ , and  $S_{\epsilon}$ , while  $\alpha$ CD40 + IL4 results in targeting of  $S_{\gamma 1}$  and  $S_{\epsilon}$ . Therefore, it is plausible that different activation conditions lead to differences in the activation rate of the 3RR enhancer region and, therefore, lead to different chromatin dynamics.

Our results suggest a possible mechanism by which 53BP1 could influence break order during CSR. Residual binding of 53BP1 to chromatin independently of DNA-damage controls *Igh* chromatin architecture ensuring a restricted contact between the  $S_{\gamma 1}$  region and the loop base containing  $S_{\mu}$  and the

that AID targeting is not affected by an absence of 53BP1 (Reina-San-Martin et al., 2007). This is expected, as the absence of 53BP1 does not impact AID expression nor does it impact the level of switch region sterile transcripts (Reina-San-Martin et al., 2007). To measure differences in DSB formation, the J. Stavnezer lab used ligation-mediated PCR (LM-PCR) and showed that an absence of 53BP1 does not affect the level of DSBs introduced at  $S_{\mu}$  (Khair et al., 2014). Furthermore,  $S_{\gamma 3}$  is targeted at the same frequency in wild-type versus 53BP1-deficient B cells undergoing switching to IgG3 in the presence of LPS. Unfortunately, assessment of breaks in  $S_{\gamma 1}$  is hindered by its length and repetitiveness. These findings suggest that, although 53BP1 is important for determining where the first break is introduced, the level of DSBs at these sites is not altered.

A recent study has shown that CSR is intrinsically biased toward productive deletional events with non-productive inversional events being suppressed (Dong et al., 2015). As in our study, the mechanism underlying orientation-dependent recombination depends on 53BP1 and is independent of the ATM/ $\gamma$ H2AX pathway and resection via RIF1. The authors of this paper propose that nuclear organization of the switch regions may be responsible for establishing this mechanism. Our data support this model, as they identify a role for 53BP1 in altering the architecture of the *Igh* constant region, leading to changes in break order and the outcome of CSR.

It is unclear at this point whether the change in location of the first break has any impact on whether recombination occurs via a deletional rather than an inversional event or whether this bias is solely due to the change in chromatin configuration. However, we speculate that alterations in locus conformation that lead to higher frequency  $S_{\mu}$ - $S_{\gamma 1}$  interactions in the absence of 53BP1 favor the ligation events needed for inversional recombination. This requires that two pairs of broken ends find each other in 3D space, in contrast to deletional events that rely on only one pair of ends coming together (Figure 3C). Clearly, inversional joining events favor the introduction of breaks occurring in close proximity, and this is indeed what we detected in 53BP1-deficient cells. Thus, the four broken ends are in more frequent contact compared to wild-type cells.

Here, we have uncovered an unanticipated function for 53BP1 in controlling chromatin conformation of *Igh* independently of damage during CSR. This finding raises the question of whether 53BP1 has similar functions in altering chromatin conformation outside of the *Igh* locus, where it could protect against AID targeting and other types of DNA damage. Likely candidate regions are repeats enriched with H4K20me2 marks that act as substrates for residual binding of 53BP1. High-resolution Hi-C experiments will show whether the effect on chromatin conformation that we detected on the *Igh* locus expands to such repeat regions.

## EXPERIMENTAL PROCEDURES

For further description see the [Supplemental Experimental Procedures](#).

### Metaphase FISH Assays

Metaphase FISH analyses were performed and analyzed as previously described (Rocha et al., 2012). The probe identifying the 5' end of *Igh* was generated by labeling of BAC RP24-386J17 and the 3' of *Igh* was labeled using

BAC CT7-199M11. The  $C_{\mu}$  probe was designed using the webfish tool (Nedbal et al., 2012) ([webfish2.org](#)). These probes were amplified by PCR from genomic DNA, mixed together at equimolar amounts, and then labeled by nick translation.

### 4C-Seq

4C-seq was performed and analyzed as previously described (Raviram et al., 2016; Rocha et al., 2012). The DpnII and Csp6 enzymes were used for digestions. Mice deficient for AID (*Aicda*<sup>-/-</sup>), 53BP1 (*Trp53bp1*<sup>-/-</sup>), as well as double-deficient mice (*Trp53bp1*<sup>-/-</sup>;*Aicda*<sup>-/-</sup>) were generated by breeding double heterozygous *Trp53bp1*<sup>+/-</sup>;*Aicda*<sup>+/-</sup> mice. The *53bp1*<sup>+/-</sup>;*Aicda*<sup>+/-</sup> mice also were generated from this breeding scheme and used as controls. 4C-seq libraries were produced by PCR amplification using primers containing Illumina single-read adaptors, barcodes for lane multiplexing, and the following *Igh* E $\mu$ -specific sequence: 5'-TCTGTCCTAAAGCTCTGAGATC and 5'-GAACACAGAAGTATGTGTATGGA. A total of 1  $\mu$ g DNA was amplified per sample using 30 PCR cycles.

Mapping was performed using Bowtie2 to a reduced genome consisting of all unique 24-nt-long regions surrounding DpnII sites, allowing for zero mismatches. As can be seen in Figure S3C, our strategy allows mapping of 4C reads to the whole constant region of *Igh* including the switch regions. Samples containing less than 0.6 million mapped reads (following removal of undigested and self-ligated fragments) were discarded. Additionally, samples with fewer than 0.2 *cis/trans* ratio of mapped reads and with fewer than 40% read coverage for all DpnII sites in the 200 kb surrounding the bait region were discarded, as these are considered important criteria for high-quality 4C-seq datasets.

Analysis of 4C-seq signal was performed by building successive 10-kb windows with 95% overlap and calculating the total number of reads per window. The following mm10 coordinates were used for this analysis Chr12: 113175000–113475000. For comparison between genotypes and/or conditions, DESeq2 1.10.0 with default parameters was used to normalize total read count per window between samples and to identify the windows with significant 4C signal differences, using an FDR-adjusted p value cutoff of 0.05.

### ACCESSION NUMBERS

The accession number for the 4C-seq data reported in this paper is GEO: GSE81180.

### SUPPLEMENTAL INFORMATION

Supplemental Information includes Supplemental Experimental Procedures, three figures, and three tables and can be found with this article online at <http://dx.doi.org/10.1016/j.celrep.2016.05.073>.

### AUTHOR CONTRIBUTIONS

P.P.R., Y.F., J.K., V.L., A.A., E.S., A.P., and A.B. performed experiments. P.P.R., R.R., and J.A.S. analyzed the data. E.R.M., R.B., J.P., and G.S. contributed with reagents and analytical tools. P.P.R. and J.A.S. conceived the project and wrote the manuscript with help from all authors.

### ACKNOWLEDGMENTS

We thank members of the J.A.S. lab for discussions, Alexander Nubla and New York University Medical Center (NYUMC) Division of Laboratory Animal Resources (DLAR) for mouse breeding, the NYU High Performance Computing (HPC) (Shenglong Wang) for computing technical support, and the NYUMC Genome Technology Center (GTC) core. We are also thankful to the following people who shared material with us: Frederick Alt, Michel Nussenzweig, and Barry Sleckman. This work was supported by grants from the NIH (GM59413 and P30 CA008748 to J.P. and GM086852 and GM112192 to J.A.S.) and the Deutsche Forschungsgemeinschaft (SFB684) to G.S. J.A.S.

is a Leukemia Lymphoma Society Scholar. P.P.R. is a National Cancer Center and American Society of Hematology fellow.

Received: February 23, 2016

Revised: April 27, 2016

Accepted: May 17, 2016

Published: June 16, 2016

## REFERENCES

- Bekker-Jensen, S., Lukas, C., Melander, F., Bartek, J., and Lukas, J. (2005). Dynamic assembly and sustained retention of 53BP1 at the sites of DNA damage are controlled by Mdc1/NFBD1. *J. Cell Biol.* *170*, 201–211.
- Bohgaki, M., Bohgaki, T., El Ghamrasni, S., Srikumar, T., Maire, G., Panier, S., Fradet-Turcotte, A., Stewart, G.S., Raught, B., Hakem, A., and Hakem, R. (2013). RNF168 ubiquitylates 53BP1 and controls its response to DNA double-strand breaks. *Proc. Natl. Acad. Sci. USA* *110*, 20982–20987.
- Bothmer, A., Robbiani, D.F., Di Virgilio, M., Bunting, S.F., Klein, I.A., Feldhahn, N., Barlow, J., Chen, H.T., Bosque, D., Callen, E., et al. (2011). Regulation of DNA end joining, resection, and immunoglobulin class switch recombination by 53BP1. *Mol. Cell* *42*, 319–329.
- Botuyan, M.V., Lee, J., Ward, I.M., Kim, J.E., Thompson, J.R., Chen, J., and Mer, G. (2006). Structural basis for the methylation state-specific recognition of histone H4-K20 by 53BP1 and Crb2 in DNA repair. *Cell* *127*, 1361–1373.
- Bunting, S.F., Callén, E., Wong, N., Chen, H.T., Polato, F., Gunn, A., Bothmer, A., Feldhahn, N., Fernandez-Capetillo, O., Cao, L., et al. (2010). 53BP1 inhibits homologous recombination in Brca1-deficient cells by blocking resection of DNA breaks. *Cell* *141*, 243–254.
- Callén, E., Jankovic, M., Wong, N., Zha, S., Chen, H.T., Difiilippantonio, S., Di Virgilio, M., Heidkamp, G., Alt, F.W., Nussenzweig, A., and Nussenzweig, M. (2009). Essential role for DNA-PKcs in DNA double-strand break repair and apoptosis in ATM-deficient lymphocytes. *Mol. Cell* *34*, 285–297.
- Chaudhuri, J., Khuong, C., and Alt, F.W. (2004). Replication protein A interacts with AID to promote deamination of somatic hypermutation targets. *Nature* *430*, 992–998.
- Chaumeil, J., and Skok, J.A. (2012). The role of CTCF in regulating V(D)J recombination. *Curr. Opin. Immunol.* *24*, 153–159.
- Chiarle, R., Zhang, Y., Frock, R.L., Lewis, S.M., Molinie, B., Ho, Y.J., Myers, D.R., Choi, V.W., Compagno, M., Malkin, D.J., et al. (2011). Genome-wide translocation sequencing reveals mechanisms of chromosome breaks and rearrangements in B cells. *Cell* *147*, 107–119.
- Di Noia, J.M. (2015). Molecular biology: Unequal opportunity during class switching. *Nature* *525*, 44–45.
- Di Virgilio, M., Callen, E., Yamane, A., Zhang, W., Jankovic, M., Gitlin, A.D., Feldhahn, N., Resch, W., Oliveira, T.Y., Chait, B.T., et al. (2013). Rif1 prevents resection of DNA breaks and promotes immunoglobulin class switching. *Science* *339*, 711–715.
- Dong, J., Panchakshari, R.A., Zhang, T., Zhang, Y., Hu, J., Volpi, S.A., Meyers, R.M., Ho, Y.J., Du, Z., Robbiani, D.F., et al. (2015). Orientation-specific joining of AID-initiated DNA breaks promotes antibody class switching. *Nature* *525*, 134–139.
- Dudley, D.D., Manis, J.P., Zarrin, A.A., Kaylor, L., Tian, M., and Alt, F.W. (2002). Internal IgH class switch region deletions are position-independent and enhanced by AID expression. *Proc. Natl. Acad. Sci. USA* *99*, 9984–9989.
- Feldman, S., Achour, I., Wuerffel, R., Kumar, S., Gerasimova, T., Sen, R., and Kenter, A.L. (2015). Constraints contributed by chromatin looping limit recombination targeting during Ig class switch recombination. *J. Immunol.* *194*, 2380–2389.
- Franco, S., Gostissa, M., Zha, S., Lombard, D.B., Murphy, M.M., Zarrin, A.A., Yan, C., Tepsuporn, S., Morales, J.C., Adams, M.M., et al. (2006). H2AX prevents DNA breaks from progressing to chromosome breaks and translocations. *Mol. Cell* *21*, 201–214.
- Gerasimova, T., Guo, C., Ghosh, A., Qiu, X., Montefiori, L., Verma-Gaur, J., Choi, N.M., Feeney, A.J., and Sen, R. (2015). A structural hierarchy mediated by multiple nuclear factors establishes IgH locus conformation. *Genes Dev.* *29*, 1683–1695.
- Gostissa, M., Schwer, B., Chang, A., Dong, J., Meyers, R.M., Marecki, G.T., Choi, V.W., Chiarle, R., Zarrin, A.A., and Alt, F.W. (2014). IgH class switching exploits a general property of two DNA breaks to be joined in cis over long chromosomal distances. *Proc. Natl. Acad. Sci. USA* *111*, 2644–2649.
- Gu, H., Zou, Y.R., and Rajewsky, K. (1993). Independent control of immunoglobulin switch recombination at individual switch regions evidenced through Cre-loxP-mediated gene targeting. *Cell* *73*, 1155–1164.
- Hu, J., Tepsuporn, S., Meyers, R.M., Gostissa, M., and Alt, F.W. (2014). Developmental propagation of V(D)J recombination-associated DNA breaks and translocations in mature B cells via dicentric chromosomes. *Proc. Natl. Acad. Sci. USA* *111*, 10269–10274.
- Jankovic, M., Feldhahn, N., Oliveira, T.Y., Silva, I.T., Kieffer-Kwon, K.R., Yamane, A., Resch, W., Klein, I., Robbiani, D.F., Casellas, R., and Nussenzweig, M.C. (2013). 53BP1 alters the landscape of DNA rearrangements and suppresses AID-induced B cell lymphoma. *Mol. Cell* *49*, 623–631.
- Keim, C., Kazadi, D., Rothschild, G., and Basu, U. (2013). Regulation of AID, the B-cell genome mutator. *Genes Dev.* *27*, 1–17.
- Khair, L., Guikema, J.E., Linehan, E.K., Ucher, A.J., Leus, N.G., Ogilvie, C., Lou, Z., Schrader, C.E., and Stavnezer, J. (2014). ATM increases activation-induced cytidine deaminase activity at downstream S regions during class-switch recombination. *J. Immunol.* *192*, 4887–4896.
- Klein, I.A., Resch, W., Jankovic, M., Oliveira, T., Yamane, A., Nakahashi, H., Di Virgilio, M., Bothmer, A., Nussenzweig, A., Robbiani, D.F., et al. (2011). Translocation-capture sequencing reveals the extent and nature of chromosomal rearrangements in B lymphocytes. *Cell* *147*, 95–106.
- Nedbal, J., Hobson, P.S., Fear, D.J., Heintzmann, R., and Gould, H.J. (2012). Comprehensive FISH probe design tool applied to imaging human immunoglobulin class switch recombination. *PLoS ONE* *7*, e51675.
- Nora, E.P., Lajoie, B.R., Schulz, E.G., Giorgetti, L., Okamoto, I., Servant, N., Pilot, T., van Berkum, N.L., Meisig, J., Sedat, J., et al. (2012). Spatial partitioning of the regulatory landscape of the X-inactivation centre. *Nature* *485*, 381–385.
- Oda, H., Hübner, M.R., Beck, D.B., Vermeulen, M., Hurwitz, J., Spector, D.L., and Reinberg, D. (2010). Regulation of the histone H4 monomethylase PR-Set7 by CRL4(Cdt2)-mediated PCNA-dependent degradation during DNA damage. *Mol. Cell* *40*, 364–376.
- Panier, S., and Boulton, S.J. (2014). Double-strand break repair: 53BP1 comes into focus. *Nat. Rev. Mol. Cell Biol.* *15*, 7–18.
- Rao, S.S., Huntley, M.H., Durand, N.C., Stamenova, E.K., Bochkov, I.D., Robinson, J.T., Sanborn, A.L., Machol, I., Omer, A.D., Lander, E.S., and Aiden, E.L. (2014). A 3D map of the human genome at kilobase resolution reveals principles of chromatin looping. *Cell* *159*, 1665–1680.
- Raviram, R., Rocha, P.P., Müller, C.L., Miraldi, E.R., Badri, S., Fu, Y., Swanzy, E., Proudhon, C., Snetkova, V., Bonneau, R., and Skok, J.A. (2016). 4C-ker: A Method to Reproducibly Identify Genome-Wide Interactions Captured by 4C-Seq Experiments. *PLoS Comput. Biol.* *12*, e1004780.
- Reina-San-Martin, B., Chen, H.T., Nussenzweig, A., and Nussenzweig, M.C. (2004). ATM is required for efficient recombination between immunoglobulin switch regions. *J. Exp. Med.* *200*, 1103–1110.
- Reina-San-Martin, B., Chen, J., Nussenzweig, A., and Nussenzweig, M.C. (2007). Enhanced intra-switch region recombination during immunoglobulin class switch recombination in 53BP1<sup>-/-</sup> B cells. *Eur. J. Immunol.* *37*, 235–239.
- Rocha, P.P., Micsinai, M., Kim, J.R., Hewitt, S.L., Souza, P.P., Trimarchi, T., Strino, F., Parisi, F., Kluger, Y., and Skok, J.A. (2012). Close proximity to Igh is a contributing factor to AID-mediated translocations. *Mol. Cell* *47*, 873–885.
- Santos, M.A., Huen, M.S., Jankovic, M., Chen, H.T., López-Contreras, A.J., Klein, I.A., Wong, N., Barbancho, J.L., Fernandez-Capetillo, O., Nussenzweig,

- M.C., et al. (2010). Class switching and meiotic defects in mice lacking the E3 ubiquitin ligase RNF8. *J. Exp. Med.* *207*, 973–981.
- Schotta, G., Sengupta, R., Kubicek, S., Malin, S., Kauer, M., Callén, E., Celeste, A., Pagani, M., Opravil, S., De La Rosa-Velazquez, I.A., et al. (2008). A chromatin-wide transition to H4K20 monomethylation impairs genome integrity and programmed DNA rearrangements in the mouse. *Genes Dev.* *22*, 2048–2061.
- Schrader, C.E., Bradley, S.P., Vardo, J., Mochegova, S.N., Flanagan, E., and Stavnezer, J. (2003). Mutations occur in the Ig Smu region but rarely in Sgamma regions prior to class switch recombination. *EMBO J.* *22*, 5893–5903.
- Schrader, C.E., Linehan, E.K., Mochegova, S.N., Woodland, R.T., and Stavnezer, J. (2005). Inducible DNA breaks in Ig S regions are dependent on AID and UNG. *J. Exp. Med.* *202*, 561–568.
- Sellars, M., Reina-San-Martin, B., Kastner, P., and Chan, S. (2009). Ikaros controls isotype selection during immunoglobulin class switch recombination. *J. Exp. Med.* *206*, 1073–1087.
- Stavnezer, J., and Schrader, C.E. (2014). IgH chain class switch recombination: mechanism and regulation. *J. Immunol.* *193*, 5370–5378.
- Thomas-Claudepierre, A.S., Robert, I., Rocha, P.P., Raviram, R., Schiavo, E., Heyer, V., Bonneau, R., Luo, V.M., Reddy, J.K., Borggreffe, T., et al. (2016). Mediator facilitates transcriptional activation and dynamic long-range contacts at the IgH locus during class switch recombination. *J. Exp. Med.* *213*, 303–312.
- Wuerffel, R., Wang, L., Grigera, F., Manis, J., Selsing, E., Perlot, T., Alt, F.W., Cogne, M., Pinaud, E., and Kenter, A.L. (2007). S-S synapsis during class switch recombination is promoted by distantly located transcriptional elements and activation-induced deaminase. *Immunity* *27*, 711–722.
- Zhang, T., Franklin, A., Boboila, C., McQuay, A., Gallagher, M.P., Manis, J.P., Khamlichi, A.A., and Alt, F.W. (2010). Downstream class switching leads to IgE antibody production by B lymphocytes lacking IgM switch regions. *Proc. Natl. Acad. Sci. USA* *107*, 3040–3045.

Cell Reports, Volume 16

## Supplemental Information

### **A Damage-Independent Role for 53BP1 that Impacts Break Order and *Igh* Architecture during Class Switch Recombination**

**Pedro P. Rocha, Ramya Raviram, Yi Fu, JungHyun Kim, Vincent M. Luo, Arafat Aljoufi, Emily Swanzey, Alessandra Pasquarella, Alessia Balestrini, Emily R. Miraldi, Richard Bonneau, John Petrini, Gunnar Schotta, and Jane A. Skok**

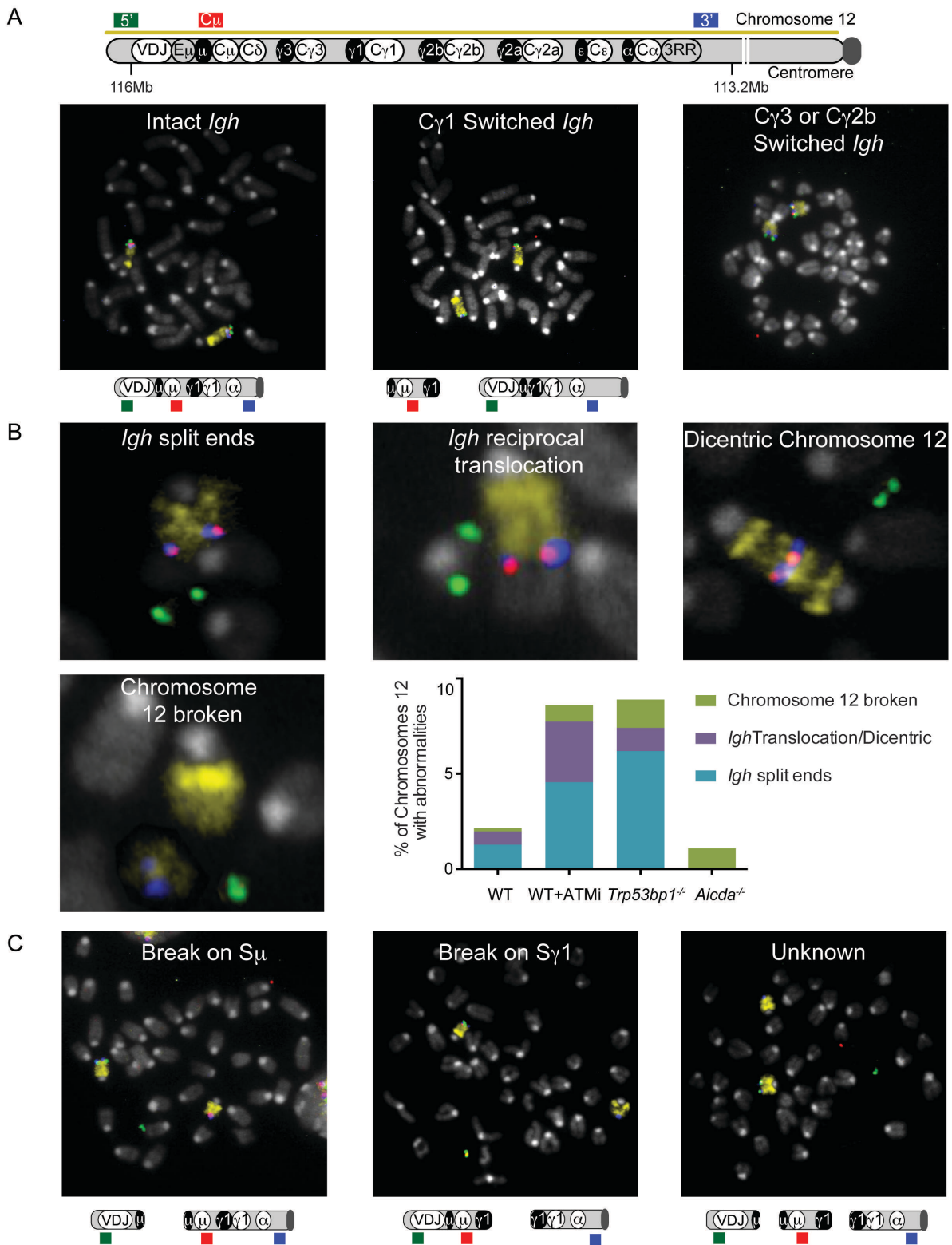


**Figure S1. Examples of switching, chromosomal abnormalities and DSB break order.**

**Related to Figure 1 and 2.**

(A) Scheme of the *Igh* locus on mouse chromosome 12 showing the location of the differentially labeled probes used in metaphase-FISH analyses (Top panel). Cells used in **Figure 1** showing examples of intact, *Cγ1* as well as *Cγ3/Cγ2b* switched *Igh* alleles (bottom

panel). **(B)** Examples of chromosomal abnormalities identified in activated B cells. Plot represents the average frequency of each chromosomal defect across replicate experiments. The percentage was calculated as a proportion of the total number of mouse chromosomes 12 analyzed (see **Table S2** for details). **(C)** Cells used in **Figure 1** and **2** showing examples of *Igh* alleles with breaks introduced first in  $S_{\mu}$ ,  $S_{\gamma 1}$  or the category classified as 'Unknown'.

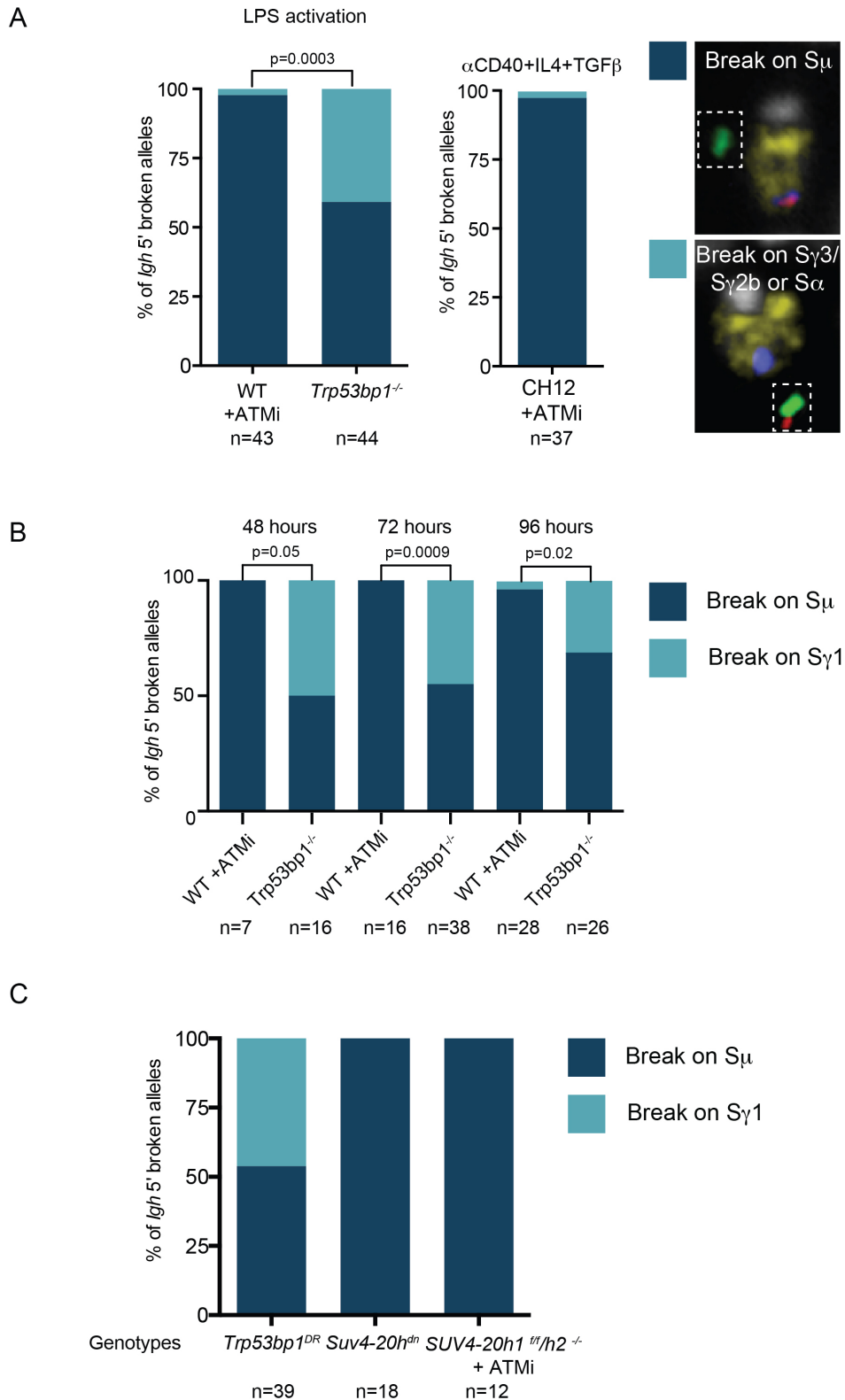


**Figure S2. Dynamics of break introduction in different activation conditions and in cells deficient for H4K20me2/m3 or deficient for 53BP1 Tudor domain.**

**Related to Figure 2.**

*Igh* alleles where location of the first break can be determined were divided into break first on S $\mu$  or S $\gamma$ 1 (or S $\gamma$ 2b/S $\alpha$ ) categories for the different mutants or treatments. Significance was

calculated using Fisher's exact test. **Table S3** details the number of replicates and alleles analyzed. Plots represent the average frequency of each category across replicate experiments. The amount of *Igh* alleles where break order could be determined is represented by n. **(A)** Metaphase analysis of WT and 53BP1 deficient cells treated with LPS for 72 hours. CH12 cells were treated for 48 hours with  $\alpha$ CD40, IL4 and TGF- $\beta$ . Broken signals were placed next to chromosome of origin for clarity **(B)** Metaphase analysis of WT cells treated with ATMi and 53BP1 deficient B cells. Cells were culture for either 48, 72 or 96 hours with  $\alpha$ CD40 and IL4. **(C)** Metaphase analysis of B cells originating from mice carrying the 53BP1DR mutation and mice deficient for SUV4-20H enzymes. As a control, cells deficient in both SUV4-20H enzymes (*Suv4-20<sup>dn</sup>*) were compared to cells carrying an intact copy of SUV4-20H1 (*Suv4-20h1<sup>ff</sup>/h2<sup>-/-</sup>*) that were treated with ATMi to increase the frequency of *Igh* chromosomal abnormalities.

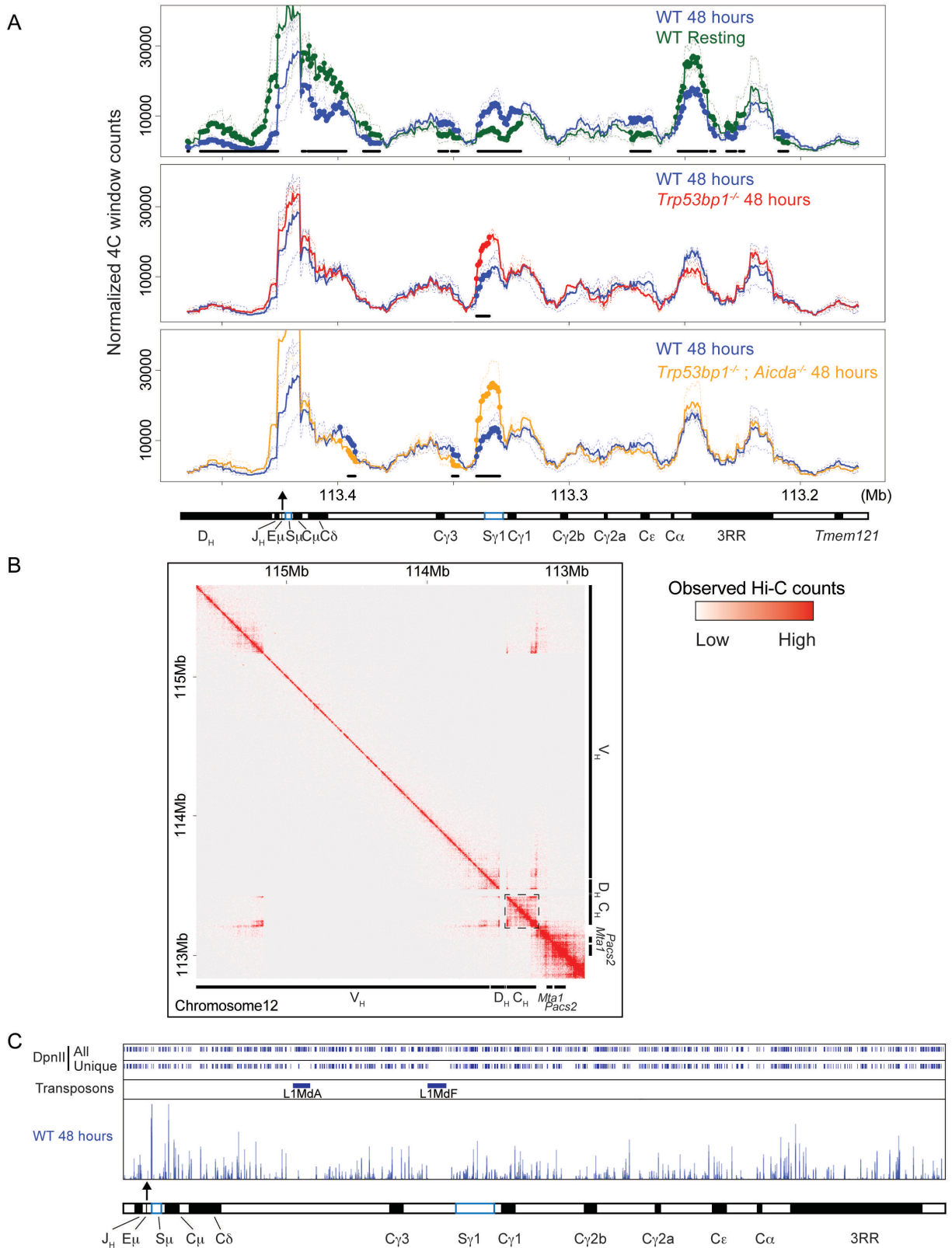


**Figure S3 Dynamics of *Igh* chromatin organization during CSR.**

**Related to Figure 3.**

(A) 4C-Seq using a bait (black arrow) located on the  $E_\mu$  enhancer. Lines represent the average 4C-signal across replicates. Dashed lines represent the signal from each replicate.

Colored circles represent windows that are significantly different (adjusted p-value < 0.05) for the two comparisons shown. For easier visualization black bars below the lines represent consecutive windows that are statistically different for the two conditions shown. For simplicity only  $\mu$  and  $\gamma 1$  switch regions are shown. **(B)** Hi-C data from the CH12 in situ combined track described in (Rao et al., 2014). Dashed square represents the *Igh* constant region ( $C_H$ ), which is insulated from interactions with genes downstream of *Igh* and with the  $D_H$  and  $V_H$  regions. **(C)** Mappability of the *Igh* constant region. Top panel shows all 24bp fragments surrounding DpnII sites across the *Igh* constant region in the mm10 genome. The second panel shows the unique fragments flanking DpnII sites on the *Igh* constant region that are used for mapping. Third panel shows the location of transposable elements, which are repetitive regions that cannot be used for 4C-Seq mapping. Bottom panel shows raw 4C-seq signal demonstrating how most of the *Igh* constant region can be mapped using 4C-Seq including the switch regions.

**Table S1. Percentage of cells expressing IgG1 as measured by FACS and by metaphase-FISH analysis.**

**Related to Figure 1.**

The increased frequency of switching identified by metaphases is likely related to the fact that some cells identified as switched might have only recombined the unrearranged V(D)J *Igh* allele. Cells with one or two C $\mu$  probes deleted were both classified as switched. Switching was measured after 72 hours of activation.

Genotype (n)	FACS (%)	Metaphases (%)
WT (9)	19.9 $\pm$ 3.8	21.5 $\pm$ 10.5
<i>Aicda</i> <sup>-/-</sup> (2)	0%	0%

**Table S2. Chromosomal abnormalities upon activation.**

**Related to Figure 1.**

Percentage represents the sum of chromosomal defects observed in each replicate divided by the total number of chromosomes 12 analyzed.

	WT			WT+ATMi			<i>Trp53bp1</i> <sup>-/-</sup>			<i>Aicda</i> <sup>-/-</sup>		
	rep1	rep2	%	rep1	rep2	%	rep1	rep2	%	rep1	rep2	%
<i>Igh</i> split ends	9	13	1.4	42	21	4.6	86	47	6.2	0	0	0
<i>Igh</i> Translocation / Dicentric	5	6	0.7	30	14	3.2	19	7	1.2	0	0	0
Chromosome 12 broken	2	1	0.2	7	5	0.9	13	19	1.5	2	1	1.1
Total Chromosomes 12	756	818		806	578		1194	956		124	154	

**Table S3. Analysis of the location of the first break.****Related to Figures 2 and 3.**

Percentage of first break in  $S_{\mu}$  or  $S_{\gamma 1}$  is calculated by summing the occurrence for each category across all replicates and dividing by the sum of all alleles across replicates where the location of the first break can be determined (Total DSB origin - this represents n in the figures). Unknown refers to *Igh* alleles where break location cannot be determined and its percentage is calculated in comparison to all *Igh* alleles identified with broken ends (Total Split *Igh*). The Total Split *Igh* category is the result of the sum of Total DSB Origin and Unknown categories. The Total *Igh* alleles category refers to the total number of chromosomes 12 analyzed for each replicate.

<b>WT + DMSO</b>	rep1	rep2	rep3	rep4	rep5	rep6	rep7	rep8	rep9	%
Break $S_{\mu}$	2	8	1	0	0	0	6	0	1	94.7
Break $S_{\gamma 1}$	0	1	0	0	0	0	0	0	0	5.3
Total DSB Origin	2	9	1	0	0	0	6	0	1	
Unknown	7	4	0	1	1	0	1	0	2	45.7
Total Split <i>Igh</i>	9	13	1	1	1	0	7	0	3	
Total <i>Igh</i> alleles	756	818	908	372	424	271	1280	786	2	

<b><i>Atm</i><sup>-/-</sup></b>	rep1	rep2	%
Break $S_{\mu}$	27	25	96.3
Break $S_{\gamma 1}$	2	0	3.7
Total DSB Origin	29	25	
Unknown	11	2	19.4
Total Split <i>Igh</i>	40	27	
Total <i>Igh</i> alleles	450	294	

<b>WT + ATMi</b>	rep1	rep2	rep3	rep4	rep5	rep6	rep7	rep8	%
Break $S_{\mu}$	18	11	24	7	9	10	8	0	94.6
Break $S_{\gamma 1}$	0	0	0	2	1	2	0	0	5.4
Total DSB Origin	18	11	24	9	10	12	8	0	
Unknown	24	10	17	2	2	1	2	0	38.7
Total Split <i>Igh</i>	42	21	41	11	12	13	10	0	
Total <i>Igh</i> alleles	806	578	3274	494	728	418	732	220	

<b><i>Trp53bp1</i><sup>-/-</sup></b>	rep1	rep2	rep3	rep4	rep5	%
Break $S_{\mu}$	18	20	7	4	39	46.6
Break $S_{\gamma 1}$	41	13	9	4	34	53.4
Total DSB Origin	59	33	16	8	73	
Unknown	27	14	10	6	69	40.0
Total Split <i>Igh</i>	86	47	26	14	142	
Total <i>Igh</i> alleles	1194	956	946	440	3972	

<b>WT+ATMi (LPS)</b>	rep1	rep2	%
Break S $\mu$	16	26	97.7
Break S $\gamma$ 1	1	0	2.3
Total DSB Origin	17	26	
Unknown	4	10	24.6
Total Split <i>Igh</i>	21	36	
Total <i>Igh</i> alleles	352	1690	
<b><i>Trp53bp1</i><sup>-/-</sup> (LPS)</b>	rep1	rep2	%
Break S $\mu$	13	13	59.1
Break S $\gamma$ 1	10	8	40.9
Total DSB Origin	23	21	
Unknown	7	5	21.4
Total Split <i>Igh</i>	30	26	
Total <i>Igh</i> alleles	1456	1480	
<b>CH12 +ATMi</b>	rep1		%
Break S $\mu$	36		97.3
Break S $\gamma$ 1	1		2.7
Total DSB Origin	37		
Unknown	5		11.9
Total Split <i>Igh</i>	42		
Total <i>Igh</i> alleles	788		
<b><i>Nbs1</i><sup>hypo</sup></b>	rep1	rep2	%
Break S $\mu$	15	4	82.6
Break S $\gamma$ 1	4	0	17.4
Total DSB Origin	19	4	
Unknown	23	14	61.7
Total Split <i>Igh</i>	42	18	
Total <i>Igh</i> alleles	2468	1330	
<b><i>H2afx</i><sup>-/-</sup></b>	rep1	rep2	%
Break S $\mu$	36	13	92.5
Break S $\gamma$ 1	4	0	7.5
Total DSB Origin	40	13	
Unknown	19	2	28.4
Total Split <i>Igh</i>	59	15	
Total <i>Igh</i> alleles	1422	311	
<b>DNA PKi +ATMi</b>	rep1	rep2	%
Break S $\mu$	14	13	90.0
Break S $\gamma$ 1	1	2	10.0
Total DSB Origin	15	15	
Unknown	7	17	44.4
Total Split <i>Igh</i>	22	32	
Total <i>Igh</i> alleles	648	394	

<b><i>Rif1</i><sup>-/-</sup></b>	rep1	rep2	%
Break S <sub>μ</sub>	43	51	83.9
Break S <sub>γ1</sub>	7	11	16.1
Total DSB Origin	50	62	
Unknown	14	19	22.8
Total Split <i>Igh</i>	64	81	
Total <i>Igh</i> alleles	3482	2966	
<b><i>Trp53bp1</i><sup>-/-</sup> + ATMi</b>	rep1	rep2	%
Break S <sub>μ</sub>	10	11	33.9
Break S <sub>γ1</sub>	32	9	66.1
Total DSB Origin	42	20	
Unknown	19	7	29.5
Total Split <i>Igh</i>	61	27	
Total <i>Igh</i> alleles	746	542	
<b><i>53BP1</i><sup>DR</sup></b>	rep1	rep2	%
Break S <sub>μ</sub>	8	13	53.8
Break S <sub>γ1</sub>	6	12	46.2
Total DSB Origin	14	25	
Unknown	11	19	42.9
Total Split <i>Igh</i>	25	44	
Total <i>Igh</i> alleles	2146	1316	
<b><i>Suv4-20h</i><sup>dn</sup></b>	rep1	rep2	%
Break S <sub>μ</sub>	8	10	100.0
Break S <sub>γ1</sub>	0	0	0.0
Total DSB Origin	8	10	
Unknown	2	1	14.3
Total Split <i>Igh</i>	10	11	
Total <i>Igh</i> alleles	605	417	
<b><i>Suv4-20h1</i><sup>trf/h2</sup><sup>+/-</sup> +ATMi</b>	rep1	rep2	%
Break S <sub>μ</sub>	5	7	100.0
Break S <sub>γ1</sub>	0	0	0.0
Total DSB Origin	5	7	
Unknown	1	1	14.3
Total Split <i>Igh</i>	6	8	
Total <i>Igh</i> alleles	806	600	

## Supplemental Experimental Procedures

### Mice

All mice used have been previously described. Mice deficient for: AID (Muramatsu et al., 2000), ATM (Barlow et al., 1996), 53BP1 (Ward et al., 2003) and H2AX (Bassing et al., 2003) as well as mice expressing the 53BP1<sup>DR</sup> (Bothmer et al., 2011) and NBS1<sup>hypo</sup> (Williams et al., 2002) proteins were derived from heterozygous or homozygous breeding of mice carrying the original mutation. As previously described (Di Virgilio et al., 2013), mice deficient for RIF1 were derived from breedings of mice carrying a floxed *Rif1* allele and mice with the *Cd19*<sup>Cre</sup> knock-in mutation. B cells deficient for both SUV420H enzymes were obtained by breeding of a mouse line carrying a *Suv420h2* homozygous deletion and floxed *Suv420h1* loci together with mice expressing the *Vav*<sup>Cre</sup> transgene (Schotta et al., 2008). Control animals for this experiment were chosen based on absence of the *Vav*<sup>Cre</sup> allele, which leads to expression of only the SUV420H1 enzyme, which is able to compensate for the H2 deficiency (Schotta et al., 2008). We refer to these control cells as *Suv4-20h1*<sup>ff/h2</sup><sup>-/-</sup> and cells carrying the *Vav*<sup>Cre</sup> transgene are *Suv4-20*<sup>dn</sup>. Animal care was approved by Institutional Animal Care and Use Committee. Protocols number is 150606-01 (NYU School of Medicine). Young mice of less than 12 weeks were used in all experiments.

### B cell activation

Splenic B cells were purified as previously described (Rocha et al., 2012). For switching to IgG1, cells were plated at  $0.25 \times 10^6$  cells/ml in RPMI 10% FCS and activated with 5ng/ml of IL4 (Sigma) and 1 $\mu$ g/ml of  $\alpha$ CD40 (Bioexcell). LPS activation to IgG2b and IgG3 was performed using a concentration of 25ng/ml. CH12 cells were grown on the same media supplemented with NCTC-109 and activation media supplemented with TGF- $\beta$  (0.1ng/ml) (Life Technologies), 5ng/ml of IL4 (Sigma) and 1 $\mu$ g/ml of  $\alpha$ CD40 (Bioexcell). ATM kinase inhibition was performed with the KU-55933 (Fisher) inhibitor at 5mM. This was added 24 and 48 hours post activation. DNA PK inhibitor (NU7441-Tocris) was administrated at 1mM also at 24 and 48 hours post activation. Cells were collected at 60-65 hours after activation for metaphase analyses except for **Figure S2** where the following time points were used (48, 72, 96). For 4C-Seq assays cells were collected 48 hours after activation to ensure cells were activated but had not yet undergone DNA excision. As a quality control switching efficiency was assessed by FACS for each experiment following 72 hours of activation.

## Metaphase FISH Assays

The following primer pairs (in 5' to 3' orientation) were used for amplification of the C<sub>μ</sub> probe:  
GGCTAAGTGAGCCAGATTGTGCTGGG and AGCCCTGTGTCCTCAGCCCC;  
TGGGGCTGAGGACACAGGGC and GCTCTGCTCTGCAGAAGGGGAAAAACC;  
GCAGCTTCCACTTCAGTCCTAGCCC and ACTTCACCTGCCAGAGAGCCG;  
ACTTCACGGCTCTCTGGCAGG and TGCTTGTAGGGGGAGGGAGC ;  
TAGCTGACCAGCTCCCCTGGC and ACAGGGGGCCACTAATCATGCC.

## Supplemental References

- Barlow, C., Hirotsune, S., Paylor, R., Liyanage, M., Eckhaus, M., Collins, F., Shiloh, Y., Crawley, J.N., Ried, T., Tagle, D., *et al.* (1996). Atm-deficient mice: a paradigm of ataxia telangiectasia. *Cell* **86**, 159-171.
- Bassing, C.H., Suh, H., Ferguson, D.O., Chua, K.F., Manis, J., Eckersdorff, M., Gleason, M., Bronson, R., Lee, C., and Alt, F.W. (2003). Histone H2AX: a dosage-dependent suppressor of oncogenic translocations and tumors. *Cell* **114**, 359-370.
- Bothmer, A., Robbiani, D.F., Di Virgilio, M., Bunting, S.F., Klein, I.A., Feldhahn, N., Barlow, J., Chen, H.T., Bosque, D., Callen, E., *et al.* (2011). Regulation of DNA end joining, resection, and immunoglobulin class switch recombination by 53BP1. *Mol Cell* **42**, 319-329.
- Di Virgilio, M., Callen, E., Yamane, A., Zhang, W., Jankovic, M., Gitlin, A.D., Feldhahn, N., Resch, W., Oliveira, T.Y., Chait, B.T., *et al.* (2013). Rif1 prevents resection of DNA breaks and promotes immunoglobulin class switching. *Science* **339**, 711-715.
- Muramatsu, M., Kinoshita, K., Fagarasan, S., Yamada, S., Shinkai, Y., and Honjo, T. (2000). Class switch recombination and hypermutation require activation-induced cytidine deaminase (AID), a potential RNA editing enzyme. *Cell* **102**, 553-563.
- Rao, S.S., Huntley, M.H., Durand, N.C., Stamenova, E.K., Bochkov, I.D., Robinson, J.T., Sanborn, A.L., Machol, I., Omer, A.D., Lander, E.S., *et al.* (2014). A 3D map of the human genome at kilobase resolution reveals principles of chromatin looping. *Cell* **159**, 1665-1680.
- Rocha, P.P., Micsinai, M., Kim, J.R., Hewitt, S.L., Souza, P.P., Trimarchi, T., Strino, F., Parisi, F., Kluger, Y., and Skok, J.A. (2012). Close proximity to Igh is a contributing factor to AID-mediated translocations. *Mol Cell* **47**, 873-885.
- Schotta, G., Sengupta, R., Kubicek, S., Malin, S., Kauer, M., Callen, E., Celeste, A., Pagani, M., Opravil, S., De La Rosa-Velazquez, I.A., *et al.* (2008). A chromatin-wide transition to H4K20 monomethylation impairs genome integrity and programmed DNA rearrangements in the mouse. *Genes Dev* **22**, 2048-2061.
- Ward, I.M., Minn, K., van Deursen, J., and Chen, J. (2003). p53 Binding protein 53BP1 is required for DNA damage responses and tumor suppression in mice. *Mol Cell Biol* **23**, 2556-2563.
- Williams, B.R., Mirzoeva, O.K., Morgan, W.F., Lin, J., Dunnick, W., and Petrini, J.H. (2002). A murine model of Nijmegen breakage syndrome. *Curr Biol* **12**, 648-653.